ORIGINAL PAPER

Reconstruction of hydrometeorological time series and its uncertainties for the Kaidu River Basin using multiple data sources

Xuemei Li · Lanhai Li · Xixi Wang · Fengqing Jiang

Abstract This paper tried to reconstruct the time series (TS) of monthly average temperature (MAT), monthly accumulated precipitation (MAP), and monthly accumulated runoff (MAR) during 1901–1960 in the Kaidu River Basin using the Delta method and the three-layered feed forward neural network with backpropagation algorithm (TLBP-FFNN) model. Uncertainties in the reconstruction of hydrometeorological parameters were also discussed. Available monthly observed hydrometeorological data covering the period 1961–2000 from the Kaidu River Basin, the monthly observed meteorological data from three stations in Central Asia, monthly grid climatic data from the Climatic Research Unit (CRU), and Coupled Model Intercomparison Project Phase 3 (CMIP3) dataset covering the period 1901–2000 were used for the reconstruction. It was found that the Delta method performed very well for calibrated and verified MAT in the Kaidu River Basin based on the monthly observed meteorological data from Central Asia, the monthly grid climatic data from CRU, and the CMIP3 dataset from 1961 to 2000. Although calibration and verification of MAP did not perform as well as MAT, MAP at Bayinbuluke station, an alpine meteorological station, showed a satisfactory result based on the data from CRU and CMIP3, indicating that the Delta method can be applied to reconstruct MAT in the Kaidu River Basin on the basis of the selected three data sources and MAP in the mountain area based on CRU and CMIP3. MAR at Dashankou station, a hydrological gauge station on the verge of the Tianshan Mountains, from 1961 to 2000 was well calibrated and verified using the TLBP-FFNN model with structure (8,1,1) by taking MAT and MAP of four meteorological stations from observation; CRU and CMIP3 data, respectively, as inputs; and the model was expanded to reconstruct TS during 1901–1960. While the characteristics of annual periodicity were depicted well by the TS of MAT, MAP, and MAR reconstructed over the target stations during the period 1901–1960, different high frequency signals were captured also. The annual average temperature (AAT) show a significant increasing trend during the 20th century, but annual accumulated precipitation (AAP) and annual accumulated runoff (AAR) do not. Although some uncertainties exist in the hydrometeorological reconstruction, this work should provide a viable reference for studying long-term change of climate and water resources as well as risk assessment of flood and drought in the Kaidu River Basin, a region of fast economic development.

X. Li · L. Li (✉) · X. Wang · F. Jiang
State Key Laboratory of Desert and Oasis Ecology,
Xinjiang Institute of Ecology and Geography,
Chinese Academy of Sciences,
818 South Beijing Road,
Urumqi, Xinjiang 830011, China
e-mail: lilh@ms.xjb.ac.cn

X. Li
Graduate School, Chinese Academy of Sciences,
Beijing 100049, China

X. Wang
Department of Civil and Environmental Engineering,
Frank Batten College of Engineering and Technology,
Old Dominion University,
Norfolk, VA 23529-0241, USA

1 Introduction

Climatic conditions play a fundamental role in shaping the environment, which are usually simulated using computer simulation models (Ninyerola et al. 2000; Jeffrey et al. 2001). These models require climate data for efficiently modeling a wide variety of environmental processes. While the nature of individual models may vary depending on data availability, most have the fundamental requirement of a dataset that is complete on a spatial and/or temporal basis (Chapman and Thornes 2003; Marquinez et al. 2003;

Skirvin et al. 2003). Facts on past climate are critical for discovering the background and variability of natural climate (Wu et al. 2010). The length and continuity of climate data series are preconditions for studying climate change. Although the 20th century may be considered as the warmest century of the last 1,000 years in the world or the Northern hemisphere, uncertainty still exists on the warming in the whole 20th century in a few parts of the earth, such as in Northwestern China. The climate in Northwest China experienced a shift from warm-dry to warm-wet in the middle of 1980s (Shi et al. 2002). For Xinjiang, a typical mountain–basin system that lies in the semiarid and arid areas of Northwest China, temperature, precipitation, and streamflow had increased obviously during the past 50 years in most parts of Xinjiang. Climate change also significantly influenced streamflow of rivers located at the southern slope of Tianshan Mountain (Chen et al. 2009; Wu et al. 2010; Tao et al. 2011; Li et al. 2011a and b). Unfortunately, the recorded meteorological and hydrological data in Xinjiang prior to the 1950 are seldom available (Fang et al. 2011). Consequently, there is no exact and believable answer whether the time scale of climate or streamflow change is decadal or centennial. The shortage of instrumental records limits the ability to assess long-term climate change and its impacts on water resources, ecosystem, and agriculture. In addition, Xinjiang is staying at an economy-booming period, which requires a better understanding on carrying capacity of water resources under climate change in the region. In the past decades, many studies focused on reconstructing local climate variability by applying climatic proxy data including historical documents, tree-rings, fossil pollens, ice cores, and lake sediment cores (Bradley and Jones 1992; Shen et al. 2001; Esper et al. 2002; Yang et al. 2002; Fang et al. 2011). However, few studies focus on drawing upon longer-term data available at nearby locations to study climate variability in Xinjiang. In its neighboring region, Central Asia, the period of instrumental monitoring starts from the 1900s or before for some stations. Meanwhile, interpolated station data such as CRU data and global climate model (GCM) data also provide historical climate data about 100 years or more. Available data offer an opportunity to hindcast the historical climate data referring to the station data from neighboring region on the correlation theory between two neighboring climate variable fields or the grid data from CRU and GCMs.

Based on the assessment of the relations between existing station data from the Kaidu River Basin and three sources of data including station data from Central Asia, CRU, and GCMs data, this paper attempts to reconstruct the historical monthly temperature and precipitation time series (TS) in the Kaidu River Basin during 1901–1960 using the Delta method. To reproduce the hydrological behavior of the Basin, a three-layered feed forward neural network with backpropagation

algorithm (TLBP-FFNN) is trained and tested with observed monthly temperature, precipitation, and runoff data from 1958 to 2002. Furthermore, the optimal combination of reconstructed temperature and precipitation during 1901–1960 is used as inputs for the TLBP-FFNN to reconstruct the monthly runoff data. The uncertainty of reconstruction is also assessed. The extension of the climate data series will provide a viable reference for studying long-term change of climate and water resources.
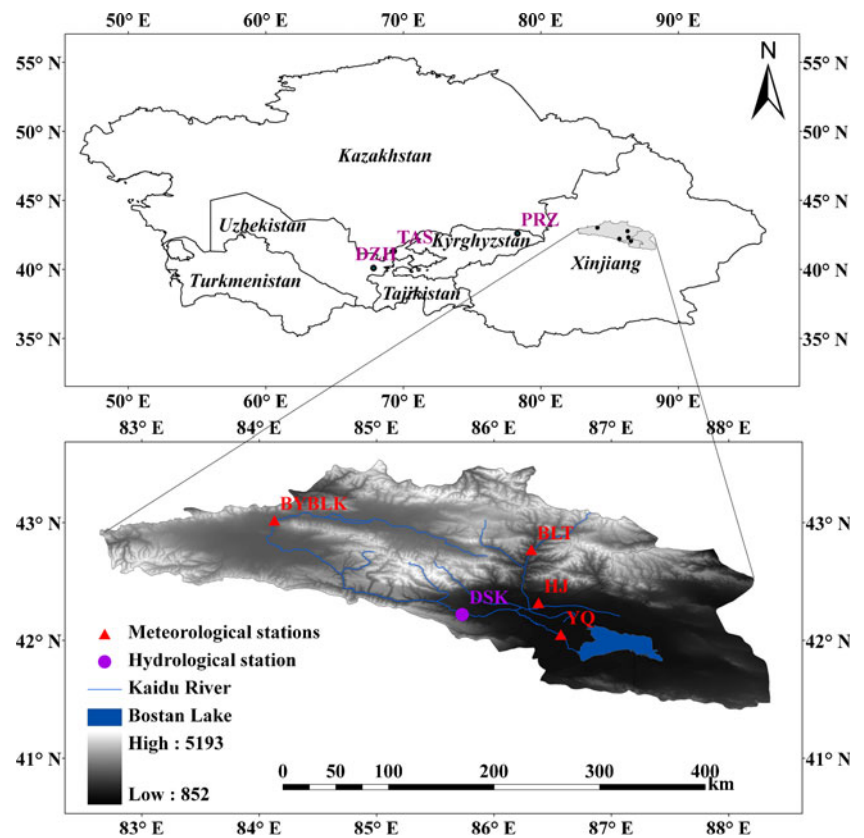
2 Study region and data

2.1 Study region

The Kaidu River is situated at the north fringe of the Yanqi Basin on the south slope of Tianshan Mountains in Xinjiang and extends from 42° 43′ to 43° 21′ N and from 82° 58′ to 86° 05′ E. It originates from the Hargat Valley and the Jacsta Valley in Sarming Mountain with a maximum altitude of 5,000 m and drains into Bosten Lake, which is located in the Bohu county of Xinjiang (Fig. 1). The records of meteorological parameters started in the late 1950s in the basin. Based on available instrumental data, the average annual temperature and the extreme minimum temperature are −4.26 °C and −48.1 °C, respectively. The annual snow-covered days are 139.3 days and the largest average annual snow depth is 12 cm (Xu et al. 2008). The mean annual, summer, and autumn temperatures as well as winter precipitation significantly increased during the period of 1958–2007 with the rates of 0.26 °C/10a, 0.28 °C/10a, 0.35 °C/10a and 1.34 mm/10a, respectively (Li et al. 2011b).

The water flows out from the other side of the lake where another river, i.e., the Kongque River, immediately starts and extends to the Tarim River. The river finally disappears in the desert. The basin is poorly gauged. Dashankou hydrological station at 1,340 m above sea level and Bayinbuluke meteorological station at 2,450 m above sea level are only two field stations with long TS data. The catchment area of the river above Dashankou station is 18,827 km², with an average elevation of 3,100 m (Tao et al. 2007). Snowmelt is not only the main water source for the evolution of the Bayinbuluk grassland but also the principal source of water required for agriculture, livestock industry, and development of economy and society of these regions. The streamflow in the basin consists of snowmelt in spring and rainfall and perennial glacier melting in summer. There are two flow peaks: the first one, mainly governed by snowmelt, appears between March and April, and the second one occurs between July and August, which is mainly controlled by rainfall. The high volume of flow within a short period will bring great hazards for downstream areas with floods resulting from snowmelt event (Dou et al. 2011).

2.2 Data

In order to reconstruct historical TS of hydrometeorological variables for the Kaidu River Basin, three sources of monthly data were used: (1) observed station data, (2) CRU data, and (3) Coupled Model Intercomparison Project Phase 3 (CMIP3) data of past and current climatic conditions.

2.2.1 Station data

The target climate records for calibration and verification are the monthly average temperature (MAT) and monthly accumulated precipitation (MAP) at four stations including Bayinbuluke, Baluntai, Hejing, and Yanqi meteorological stations within the Kaidu River Basin or surrounding areas. The target hydrological data for calibration and verification is the monthly accumulated runoff (MAR) data from the Dashankou hydrological station.

Both Central Asia and Xinjiang are located in the hinterland of Asia–Europe continent and the zone of westerly circulation. Tianshan Mountain goes over Kazakhstan of Central Asia and the middle part of Xinjiang from west to east. Therefore, the climate is similar between the two regions to a certain extent. Based on the evaluation of data availability and climate similarity, three source stations located in the neighboring region, Central Asia, were used as the reference data to reconstruct hydrometeorological TS for the Kaidu River Basin. The distance between three source stations and four target stations are about 1,000–2,000 km (Fig. 1). The basic information of both target and source stations is shown in Table 1.

2.2.2 CRU data

The Climatic Research Unit (CRU), one of the leading institutions concerned with the study of natural and anthropogenic climate change, is a component of the University of East Anglia. Consisting of approximate 30 research scientists and students, the unit has developed a number of datasets, statistical software packages, and climate models which are widely used in climate research.

The CRU TS3.1 datasets cover the period 1901–2009. TS datasets are month-by-month variation in climate over the last century with a spatial resolution of 0.5°×0.5°. Its variables include cloud cover, diurnal temperature range, frost day frequency, precipitation, daily mean temperature, monthly average daily maximum temperature, vapor pressure, and wet day frequency. The gridded values of MAT and MAP were interpolated onto the four meteorological stations of the Kaidu River Basin by bilinear interpolation. These TS were used as reference data to reconstruct past climate.

Table 1 Descriptive information of the meteorological and hydrological stations used in this study

Within	Name	Coordinate		Alt (m)	Period
		Lat	Lon		
Kaidu River Basin	Bayinbuluke[a]	43°01′	84°08′	2,450	1958–2007
	Baluntai[a]	42°46′	86°19′	1,790	1958–2007
	Hejing[a]	42°19′	86°23′	1,116	1958–2007
	Yanqi[a]	42°03′	86°34′	1,060	1958–2007
	Dashankou[b]	42°13′	85°44′	1,340	1958–2007
Central Asia	Przhevalsk[a]	42°24′	78°18′	1,716	1879–1996
	Dzhizak[a]	40°07′	67°50′	344	1887–2001
	Tashkent[a]	41°20′	69°18′	477	1877–2003

Lat latitude, *Lon* longitude, *Alt* altitude

[a] Meteorological station

[b] Hydrological station

2.2.3 CMIP3 data

CMIP3 multimodel dataset was integrated by the Program for Climate Model Diagnosis and Intercomparison (PCMDI) and the World Climate Research Programme (WCRP). The data had been collected, analyzed, and provided by the National Climate Center in China. GCMs used in this multimodel dataset included NCAR_CCSM3, GFDL_CM2_0, GFDL_CM2_1, GISS_AOM, GISS_E_H, GISS_E_R, NACR_PCM1, MROC3, MROC3_H, MRI_CGCM2, MROC3_H, MRI_CGCM2, UKMO_-HADCM3, UKMO_HADGEM, CNRMCM3, IPSL_CM4, CCCMA_3-T47, CCCMA_3-T63, BCC-CM1, AP_F-GOALS1.0, MPI_ECHAM5, MIUB_ECHO_G, CSIRO_MK3, BCCR_CM2_0, and INMCM3. One source of integrated data is called CMIP3_SAM data, which was obtained by averaging data such as MAT, MAP, and so on from these 25 GCMs by simple arithmetic mean method and interpolated into grids in the land of China with spatial resolution 1°×1°. 20C3M data means the simulation experiment data of the 20th century. The gridded MAT and MAP from 20C3M data were interpolated onto the four meteorological stations of the Kaidu River Basin by bilinear interpolation. These TS were used as reference data to reconstruct past climate.

2.3 Quality control

Quality control has been undertaken for all data. It includes examination of individual station records looking for outliers using double mass curve method. Some abnormal values were identified and either corrected or removed. No TS had missing data longer than 3 months and only a small fraction of the data needed correction. The missing data were processed in the following ways: (1) for the temperature, if only 1 month had missing data, the missing data were replaced by the mean value of the data from the two preceding and the two following records, while for the precipitation, the missing data were filled by using the method in step 2 and (2) if consecutive two or more months had missing data, the missing data were estimated by simple linear correlation between its neighboring stations ($R^2 > 0.95$).

3 Methodology

Each TS dataset was divided into three parts in accordance with the three stages in the model-building process: calibration, verification, and reconstruction. The MAT, MAP, and MAR datasets during 1971–2000 were used for calibration, during 1961–1970 for verification and during 1901–1960 for reconstruction.

3.1 The reconstruction method of meteorological time series: the Delta method

Statistical downscaling methods aim to draw empirical relationships that transform large-scale features of GCMs to regional-scale variables, such as precipitation and temperature (Tripathi et al. 2006). Sophisticated statistical downscaling methods are generally classified into three groups: weather pattern schemes (Conway et al. 1996; Fowler et al. 2000), weather generators (WGs) (Mason 2004; Dubrovsky et al. 2004), and regression models (Wilby et al. 1999). Among the statistical downscaling methods, regression models are possibly most popular, including the Delta method (Hay et al. 2000; Zhao and Xu 2007; Hao et al. 2009), multiple regression models (MRMs) (Wilby et al. 1999), canonical correlation analysis (CCA) (Karl et al. 1990; Busuioc et al. 2001), singular value decomposition (SVD) (Huth 1999), artificial neural networks (ANNs) (Zorita and Storch 1999; Olsson et al. 2004), and support vector machine (SVM) (Tripathi et al. 2006). In comparison with

other statistical downscaling methods, the Delta method can deal with larger data samples easier, train faster, and implement more efficiently. The Delta method is generally introduced by text description in the prior literatures. Here, this method is extended to the climate reconstruction and formulated as follows:

$$T(x,t) = \overline{Tb(x,t)} + \left(Tr(y,t) - \overline{Tbr(y,t)} \right) \qquad (1)$$

$$P(x,t) = \Pr(y,t) \times \left(\overline{Pb(x,t)} \Big/ \overline{Pbr(y,t)} \right) \qquad (2)$$

where t denotes the month, $t=1, 2, 3, …, 12$. $T(x,t)$ and $P(x,t)$ are the reconstructed temperature and precipitation for the target location x at the tth month during the reconstruction period. $Tr(y,t)$ and $Pr(y,t)$ represent temperature and precipitation for the referenced location y at the tth month during reconstruction period. $\overline{Tb(x,t)}$ and $\overline{Tbr(y,t)}$ are mean values of temperature during the calibration period for the target location x and the referenced location y at the tth month. $\overline{Pb(x,t)}$ and $\overline{Pbr(y,t)}$ are the means of precipitation during calibration time for the target location x and the referenced location y at the tth month.

3.2 The reconstruction method of hydrological time series: the TLBP-FFNN model

ANN has gained significant attention during past decades and has been widely used in the estimation of hydrologic, climatic, and other variables. Three-layered feed forward neural network (FFNN) includes three layers: an input layer, a hidden layer, and an output layer (Fig. 2). It provides a general framework for representing nonlinear functional mapping between a set of input and output variables (Nourani et al. 2009). In a FFNN, the weighted connections feed acti-

Input Layer   **Hidden Layer**   **Output Layer**
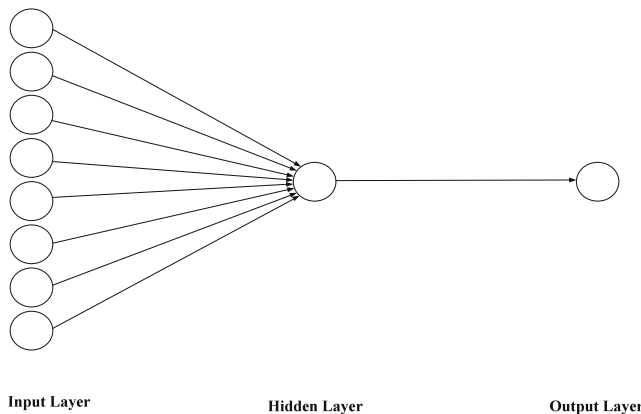
Fig. 2 The schematic diagram of a three-layered FFNN with structure (8,1,1)

vations only in the forward direction from an input layer to an output layer. On the other hand, in a recurrent network, additional weighted connections are used to feed previous activations back to the network (Srinivasulu and Jain 2006). Backpropagation (BP) network model is a feed-forward ANN structure with a BP algorithm and has proved that its three-layer structure is satisfactory for forecasting and simulating hydrology and water resources (ASCE 2000). TLBP-FFNN is often trained using the Levenberg–Marquardt (LM) algorithm as follows:

Supposing (x_i, y_i) is a set of n empirical pairs of independent and dependent variables. Parameters β of the model curve $f(x, \beta)$ is optimized so that the sum of the squares of the deviations:

$$S(\beta) = \sum_{i=1}^{n} [y_i - f(x_i, \beta)]^2 \qquad (3)$$

reaches the minimal value (Levenberg 1944; Marquardt 1963).

The input dimension and the number of hidden nodes are determined using a heuristic procedure, i.e., different inputs with increasing numbers of hidden nodes are tried (Cannas et al. 2006). The output value of TLBP-FFNN could be specifically expressed as follows:

$$\widehat{y}_k = f_0 \left[\sum_{j=1}^{n} w_{kj} \cdot f_h \left(\sum_{i=1}^{m} w_{ji} x_i + w_{jo} \right) + w_{ko} \right] \qquad (4)$$

where m and n are the number of neurons in the input layer and hidden layer, respectively ($i=1, 2, 3, …, m$ and $j=1, 2, 3, …, n$). w_{ji} and w_{kj} donate weights linking the ith neuron in the input layer with the jth neuron in the hidden layer and the jth neuron in the hidden layer with the kth neuron in the output layer, respectively. w_{jo} and w_{ko} stand for biases for the jth hidden neuron and kth neuron in the output layer, respectively. x_i represents the ith input variable for input layer and $\widehat{y}_k$ is kth computed output variable. f_h and f_o are activation functions for the hidden neuron and output neuron, respectively. Linear and Tan-sigmoid functions are popular activation functions in ANN and their general equation forms would appear as:

$$A(x) = x \qquad (5)$$

$$A(x) = \tanh \left(\frac{e^{cx} - e^{-cx}}{e^{cx} + e^{-cx}} \right) \qquad (6)$$

where $c>0$ is a positive scaling constant and x is from $-\infty$ to $+\infty$ (Vogl et al. 1988).

The TLBP-FFNN model with Tan-sigmoid activation function in the hidden neuron and linear activation

Table 2 Values of the performance measures rating, adopted from Moriasi et al. (2007)

Performance rating	Grades	NSE	RSR	PBIAS (%) MAT,MAP	MAR
Very good	A	0.75<NSE≤1	0≤RSR≤0.5	PBIAS<±15	PBIAS<±10
Good	B	0.65<NSE≤0.75	0.5<RSR≤0.6	±15≤PBIAS<±20	±10≤PBIAS<±15
Satisfactory	C	0.50<NSE≤0.65	0.6<RSR≤0.7	±20≤PBIAS<±30	±15≤PBIAS<±25
Unsatisfactory	D	NSE≤0.50	RSR>0.7	PBIAS≥±30	PBIAS≥±25

function in output neuron trained using the LM algorithm is used to model monthly runoff in this paper. The structure of $(m, n, 1)$ examines the conjunct impact of temperature and precipitation on runoff with m input variables. In the case of ANN, a data-driven statistical model, the input variables are selected from the available data, and the model is developed subsequently. For this study, the MATs and MAPs during 1961–2007 from the Bayinbuluke, Baluntai, Hejing, and Yanqi stations are available. However, the number of available variables, the correlations between potential input variables, and some variables with little or no predictive power will cause difficulty in selecting input variables (May et al. 2009).

The Akaike Information Criterion (*AIC*) (Akaike 1974) can determine the optimal number of input variables by defining the optimal trade-off between model size and accuracy by penalizing models with an increasing number of parameters. The definition of *AIC* is as follows:

$$AIC = -N \log \left(\frac{\sum_{i=1}^{N} (y_i - \widehat{y}_i)^2}{N} \right) + 2(p+1) \quad (7)$$

where y_i, $\widehat{y}_i$, N, and p are, respectively, the observed value, the predicted value, number of observations, and the number of model parameters. Here, the model accuracy and model

Table 3 Performance for calibration/verification of MAT in Kaidu River Basin based on three types of referred data using Delta method

Targeted stations	Referred stations or grids	RSR(C/V)	NSC(C/V)	PBIAS(C/V)	Performance rating
Bayinbuluke	Przhevalsk	0.16/0.14	0.97/0.98	−3.54/3.27	A/A
	Dzhizak	0.23/0.21	0.95/0.96	0.00/−4.48	A/A
	Tashkent	0.21/0.20	0.96/0.96	0.00/4.20	A/A
	Average	0.20/0.18	0.96/0.97	0.00/9.42	A/A
	CRU	0.22/0.25	0.95/0.94	−0.01/9.10	A/A
	CMIP3_20C3M	0.18/0.18	0.97/0.97	0.00/5.15	A/A
Baluntai	Przhevalsk	0.10/0.10	0.99/0.99	2.89/−0.46	A/A
	Dzhizak	0.21/0.20	0.96/0.96	−0.38/5.18	A/A
	Tashkent	0.17/0.19	0.97/0.96	−0.30/−1.38	A/A
	Average	0.16/0.15	0.98/0.98	−0.07/−5.13	A/A
	CRU	0.22/0.24	0.95/0.94	−0.07/−7.09	A/A
	CMIP3_20C3M	0.14/0.13	0.98/0.98	−0.19/−1.04	A/A
Hejing	Przhevalsk	0.11/0.11	0.99/0.99	2.00/−3.42	A/A
	Dzhizak	0.19/0.19	0.96/0.96	0.00/0.71	A/A
	Tashkent	0.17/0.19	0.97/0.96	0.00/−3.91	A/A
	Average	0.15/0.16	0.98/0.97	0.00/−6.70	A/A
	CRU	0.19/0.20	0.97/0.96	0.00/−7.41	A/A
	CMIP3_20C3M	0.13/0.13	0.98/0.98	0.00/−4.11	A/A
Yanqi	Przhevalsk	0.11/0.10	0.99/0.99	1.44/3.88	A/A
	Dzhizak	0.19/0.20	0.96/0.96	0.00/8.45	A/A
	Tashkent	0.17/0.19	0.97/0.97	0.00/3.33	A/A
	Average	0.16/0.15	0.98/0.98	0.00/0.25	A/A
	CRU	0.18/0.19	0.97/0.97	0.00/−0.29	A/A
	CMIP3_20C3M	0.12/0.12	0.98/0.99	0.00/2.90	A/A

C calibration, *V* verification

complexity are determined by the log-likelihood and the term $p+1$, respectively. Typically, the regression error decreases with increasing p, but since the model is more likely to be overfit for a fixed sample size, the increasing complexity is penalized. At some point, an optimal *AIC* is determined, which represents the optimal trade-off between model accuracy and model complexity. The optimum model is determined by minimizing the *AIC* with respect to the number of model parameters, p. The *AIC* is used to determine the optimal number of input variables in this study.

For this study, the available inputs are the MAT at times t, $t-1$, and $t-2$ (i.e., MAT (t), MAT $(t-1)$, and MAT $(t-2)$) and the MAP at times t, $t-1$, and $t-2$ (i.e., MAP (t), MAP $(t-1)$, and MAP $(t-2)$) from four target stations in the Kaidu River Basin. The only neuron in the output layer representing the runoff at time t, MAR (t), is modeled. Also, n is the number of neurons in the hidden layer in the development of the TLBP-FFNN model. Scheme of the LM BP was used as the training algorithm in Matlab Neural Network Toolbox in this study. The MAT and MAP values from calibration dataset are inputted layer neurons to calibrate the runoff 2 months forward (as output layer neuron) via the TLBP-FFNNs model. Then, the trained model was validated by the verification dataset. In TLBP-FFNNs modeling, the TLBP-FFNNs architecture and training iteration number (epoch) are important. Appropriate selection of these can progress the model efficiency in both the steps of calibration (training) and verification, and prevent the TLBP-FFNN model to be overtrained. In this study, it was realized that 10,000 epochs satisfy the training network with 10^{-4} as goal performance and no great improvements in the model performance were found when the number of hidden neurons was increased from a threshold.

3.3 The assessment indices

Nash–Sutcliffe coefficient (*NSC*) (Nash and Sutcliffe 1970), ratio of root mean square error, and observations standard deviation (*RSR*), and percentage bias (*PBIAS*) were employed as statistical indicators to evaluate the performance of calibration and verification. They are defined as follows:

$$NSC = 1 - \frac{\sum\limits_{i=1}^{N}(y_i - \widehat{y}_i)^2}{\sum\limits_{i=1}^{N}(y_i - \overline{y})^2} \qquad (8)$$

$$RSR = \frac{\sqrt{\frac{\sum\limits_{i=1}^{N}(y_i - \widehat{y}_i)^2}{N}}}{\sqrt{\frac{\sum\limits_{i=1}^{N}(y_i - \overline{y})^2}{N}}} \qquad (9)$$
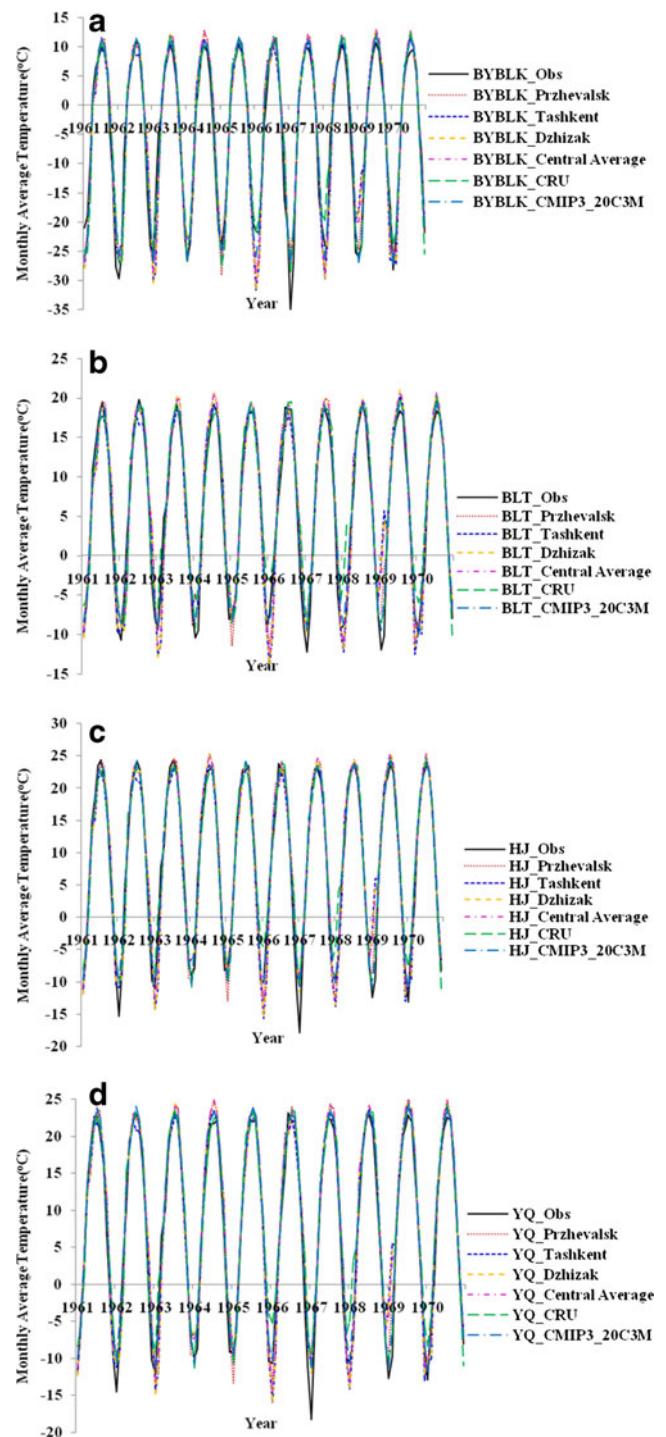
Fig. 3 The time series of observed and verified MAT using Delta method during verification period (1961–1970) in Kaidu River Basin. **a** Bayinbuluke station, **b** Baluntai station, **c** Hejing station, and **d** Yanqi station

$$PBIAS = \frac{\sum\limits_{i=1}^{N}(y_i - \widehat{y}_i) \times 100}{\sum\limits_{i=1}^{N} y_i} \qquad (10)$$

where y_i, $\widehat{y}_i$, $\overline{y}$, and N are, respectively, the observed value, the predicted value, the mean value of the observed data, and number of observations.

The theoretical range of *NSC* is from $-\infty$ to 1. *NSC* with a value greater than zero is used as an indicator to assess the agreement between observed and estimated values. When the value of *NSC* is close to 1, the estimated data series is close to the observation. *RSR* varies from the optimal value of 0, indicating perfect model simulation, to a large positive value. The lower the *RSR* and the root mean square error, the better the model simulation performance (Moriasi et al. 2007). *PBIAS* measures whether the model output is smaller or larger than the corresponding observed values and can clearly indicate the performance of a model (Gupta et al. 1999). The positive *PBIAS* indicates that the model is underestimated, and a negative one indicates that the model is overestimated (Gupta et al. 1999). The values of *NSE* greater than 0.5, value of *RSR* less than 0.7, and the absolute values of *PBIAS* less than 25 % indicate the satisfactory model performance (Table 2) (Moriasi et al. 2007).

4 Results and discussion

4.1 The performance assessment of calibrated and verified temperature

Table 3 shows the performances from calibration and verification by Delta method for MAT in the Kaidu River Basin. The results indicate that calibration and verification based on three sources of referred data generated similar performances for calibrated and verified MAT in the Kaidu River Basin. Values of *NSC*, *RSR*, and *PBIAS* indicate that all the three sources of referred data perform very well during calibration and verification of MAT. There was no large difference between calibrated and verified MAT and observed ones, but different source data performed differently. Calibrated and verified results based on grid data from CMIP3 and station data from Central Asia are better than that from CRU.

The same data sources also generate different MAT at four target stations during the calibration and verification periods. A better calibration and verification performance based on station data from Central Asia was achieved at

Table 4 Performance for calibration/verification of MAP in Kaidu River Basin based on three types of referred data using Delta method

| Targeted stations	Referred stations or grids	RSR(C/V)	NSC(C/V)	PBIAS(C/V)	Performance rating
Bayinbuluke	Przhevalsk	0.63/0.74	0.60/0.45	2.87/6.98	C/D
	Dzhizak	2.47/2.74	−5.08/−6.53	0.00/22.75	D/D
	Tashkent	2.07/2.41	−3.29/−4.79	3.84/2.08	D/D
	Average	0.78/0.80	0.39/0.35	1.46/17.71	D/D
	CRU	0.61/0.58	0.63/0.67	0.00/−1.61	C/C
	CMIP3_20C3M	0.52/0.53	0.73/0.72	0.00/−1.07	B/B
Baluntai	Przhevalsk	0.71/0.83	0.50/0.28	6.16/17.99	D/D
	Dzhizak	2.06/2.30	−3.22/−4.30	0.00/34.27	D/D
	Tashkent	1.59/2.28	−1.54/−4.21	0.40/8.86	D/D
	Average	0.78/0.85	0.39/0.28	0.17/28.57	D/D
	CRU	0.72/0.71	0.48/0.49	0.00/3.89	D/D
	CMIP3_20C3M	0.71/0.73	0.49/0.47	0.00/5.91	D/D
Hejing	Przhevalsk	0.81/0.83	0.35/0.30	−1.26/39.27	D/D
	Dzhizak	1.62/2.07	−1.65/−3.09	0.00/58.49	D/D
	Tashkent	1.33/2.55	−0.75/−5.82	3.04/38.83	D/D
	Average	0.81/0.91	0.34/0.17	1.30/53.47	D/D
	CRU	0.87/0.87	0.26/0.21	0.00/24.10	D/D
	CMIP3_20C3M	0.88/0.86	0.22/0.23	0.00/26.33	D/D
Yanqi	Przhevalsk	0.80/0.84	0.35/0.31	3.70/20.12	D/D
	Dzhizak	1.64/1.84	−1.65/−3.09	0.00/38.58	D/D
	Tashkent	1.37/2.01	−0.75/−5.81	4.62/19.94	D/D
	Average	0.82/0.90	0.34/0.17	1.98/33.37	D/D
	CRU	0.89/0.89	0.26/0.21	0.00/7.36	D/D
	CMIP3_20C3M	0.87/0.88	0.22/0.23	0.00/10.38	D/D

Baluntai, Hejing, and Yanqi stations than at Bayinbuluke station. When calibrating and verifying the data for a given target station, the data from Przhevalsk station performed much better than that from Dzhizak and Tashkent stations, as well as the mean value of temperature from Przhevalsk, Dzhizak, and Tashkent stations. The source data from CRU and CMIP3 also carried out a better performance during calibration and verification at Hejing and Yanqi stations than that at Bayinbuluke and Baluntai stations. Figure 3 shows the comparison between observed and verified MAT at four target stations during the validation period 1961–1970. It can be seen that the Delta method performs well for the four target stations based on three data sources. According to values of *PBIAS* in Table 3 and Fig. 3a and d, the MAT at Bayinbuluke and Yanqi stations are underestimated by the Delta method based on all the three sources of referred data during verification. Meanwhile, the MAT at Hejing and Yanqi stations are overestimated during verification (Table 3, Fig. 3b and c).

4.2 The performance assessment of calibrated and verified precipitation

Performances from calibration and verification of MAP by the Delta method in the Kaidu River Basin are shown in Table 4. Comparing with the calibrated and verified results of MAT, performances are poor for MAP. Values of *NSC*, *RSR*, and *PBIAS* indicate that three sources of referred data perform unsatisfactorily during calibration and verification of MAP at the Baluntai, Hejing, and Yanqi stations in the Kaidu River Basin, but Bayinbuluke station is an exception with a satisfactory result.

Similar to calibration and verification of MAT, different precipitation data sources generate different precipitation values for a given station and the same data source performs differently at different meteorological stations during the calibration and verification periods. The values of *NSC* are positive for precipitation calibration and verification based on the CRU, CMIP3 data, and station data from the Przhevalsk station and the average values from three stations of Central Asia, but negative *NSC* values exist based on station data from the Dzhizak and Tashkent stations. CMIP3 and CRU data have similar performances for calibrating and verifying MAP in the Kaidu River Basin. It can be seen clearly from the comparison between observed and verified MAP at four target stations during validation period 1961–1970 (Fig. 4).

MAP was calibrated and verified by the Delta method based on CMIP3 data, and CRU data performs satisfactory at the Bayinbuluke station. The good and satisfactory performance of calibrated and verified MAP at the Bayinbuluke station located in the mountain area indicate that CMIP3
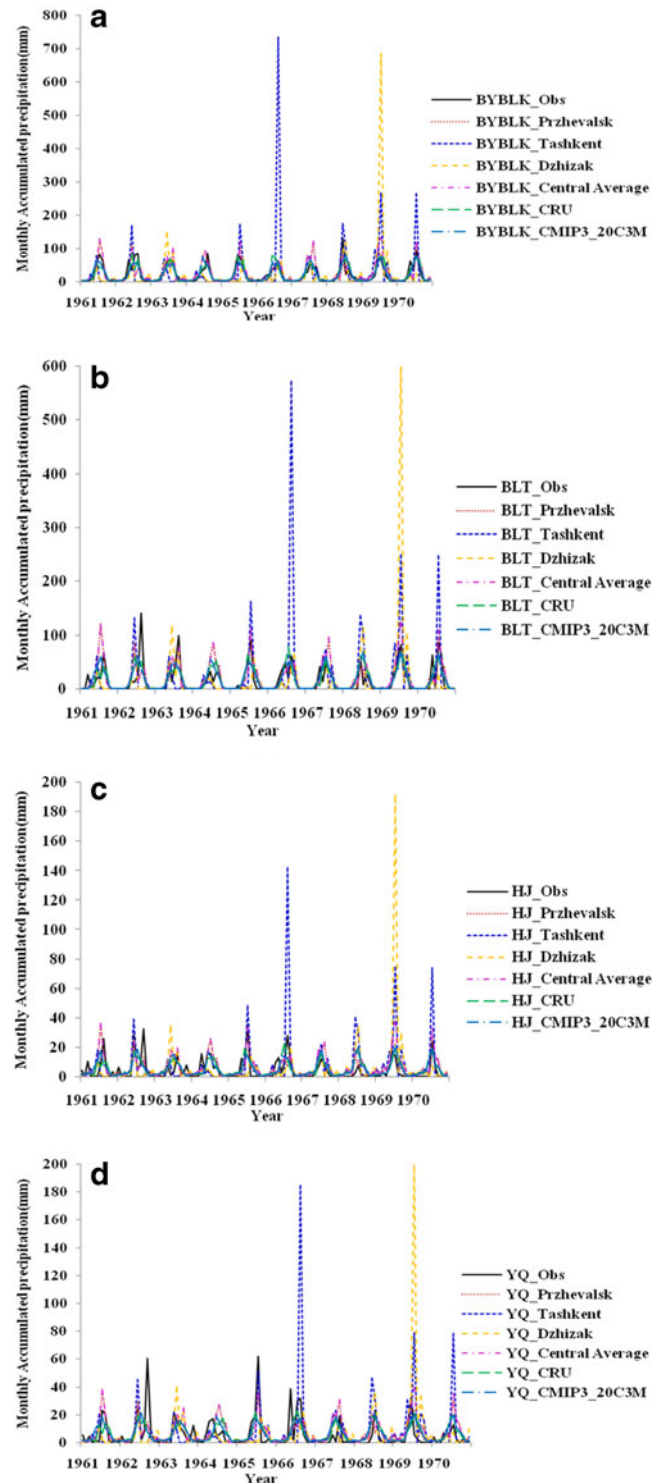
Fig. 4 The time series of observed and verified MAP using Delta method during verification period (1961–1970) in Kaidu River Basin. **a** Bayinbuluke station, **b** Baluntai station, **c** Hejing station, and **d** Yanqi station

data and CRU data can be used to reconstruct the precipitation in the mountains where the runoff generates.

Table 5 Pearson correlation coefficient between MAT from observation, CRU, and CMIP3 data and observed MAR at Dashankou station as well as that between MAP from observation, CRU, and CMIP3 data and observed MAR at Dashankou station in Kaidu River Basin

	Observed DSK_MAR	Observed DSK_MAR	Observed DSK_MAR
BYBLK_MAT	0.78** (Obs)	0.79** (CRU)	0.83** (CMIP3)
BYBLK_MAP	0.83** (Obs)	0.60** (CRU)	0.56** (CMIP3)
BLT_MAT	0.80** (Obs)	0.81** (CRU)	0.83** (CMIP3)
BLT_MAP	0.78** (Obs)	0.50** (CRU)	0.47** (CMIP3)
YQ_MAT	0.79** (Obs)	0.80** (CRU)	0.83** (CMIP3)
YQ_MAP	0.51** (Obs)	0.43** (CRU)	0.41** (CMIP3)
HJ_MAT	0.80** (Obs)	0.80** (CRU)	0.83** (CMIP3)
HJ_MAP	0.51** (Obs)	0.43** (CRU)	0.45** (CMIP3)

(*Obs*) Pearson correlation coefficient between MAT, MAP from observation data and observed DSK_MAR, (*CRU*) Pearson correlation coefficient between MAT, MAP from CRU data and observed DSK_MAR, (*CMIP3*) Pearson correlation coefficient between MAT, MAP from CMIP3 data and observed DSK_MAR

** Correlation is significant at the 0.01 confidence level (two-tailed)

The above results indicate that the Delta method performs very well and makes low uncertainty in calibration and verification of MAT based on the selected three referred data sources in four target stations from the Kaidu River Basin. It also generates good MAP based on CMIP3 data and satisfactory MAP based on CRU data at the Bayinbuluke station in the Kaidu River Basin. A possible reason is that the temperature is impacted mainly by radiation balance and easily grasped and reconstructed. However, precipitation is impacted by many factors such as local climate, topography, and vapor sources, etc. and difficult to be modeled. So it will produce less uncertainty if the selected three data sources are used to reconstruct the MAT during 1901–1960 in four target stations from the Kaidu River Basin and CMIP3 data and CRU data to reconstruct MAP at the Bayinbuluke station. In addition, the good quality of grid data from CMIP3 and CRU used in this study covering the study area can explain the better performance than station data from Central Asia in calibration and verification for precipitation of the Kaidu River Basin. Because of the long distance between three stations from Central Asia and the four target stations of the Kaidu River Basin, the station data

Table 6 Performance for calibration/verification of MAR using different structures of TLBP-FFNN model based on MAT and MAP of four meteorological stations from observation, CRU, and CMIP3 data in Kaidu River Basin

Structures	Data sources	NSC(C/V)	RSR(C/V)	PBIAS(C/V)	AIC(C/V)	Performance rating
(2,1,1)	Observation	0.79/0.81	0.46/0.49	0.00/3.22	152/238	A/A
	CRU	0.73/0.79	0.52/0.56	0.00/0.08	62/202	B/B
	CMIP3	0.72/0.81	0.53/0.57	0.00/1.26	51/231	B/B
(4,1,1)	Observation	0.84/0.83	0.41/0.43	0.00/4.58	245/291	A/A
	CRU	0.74/0.79	0.51/0.55	0.00/−0.35	73/213	B/B
	CMIP3	0.73/0.79	0.52/0.56	0.00/1.46	66/212	B/B
(6,1,1)	Observation	0.83/0.83	0.41/0.44	0.00/4.82	243/290	A/A
	CRU	0.75/0.76	0.50/0.54	0.00/−1.67	98/168	B/B
	CMIP3	0.73/0.77	0.52/0.56	0.00/−0.34	68/172	B/B
(8,1,1)	Observation	0.85/0.86	0.39/0.42	0.00/2.44	286/286	A/A
	CRU	0.74/0.74	0.51/0.54	0.00/−0.90	91/91	B/B
	CMIP3	0.73/0.74	0.52/0.56	0.00/−0.52	74/74	B/B
(16,1,1)	Observation	0.84/0.85	0.40/0.43	0.00/8.19	280/280	A/A
	CRU	0.76/0.74	0.49/0.53	0.00/−5.44	132/132	A/B
	CMIP3	0.73/0.76	0.52/0.56	0.00/2.35	94/94	B/B
(24,1,1)	Observation	0.90/0.87	0.32/0.34	0.00/3.94	462/462	A/A
	CRU	0.75/0.77	0.50/0.54	0.00/−1.20	134/134	B/B
	CMIP3	0.79/0.71	0.46/0.49	0.00/3.50	196/196	A/B

Structure (2,1,1) refers to input variables: T_BYBLK(*t*), P_BYBLK(*t*); Structure (4,1,1), T_BYBLK(*t*−1), T_BYBLK(*t*), P_BYBLK(*t*−1), P_BYBLK(*t*); Structure (6,1,1), T_BYBLK(*t*−2), T_BYBLK(*t*−1), T_BYBLK(*t*), P_BYBLK(*t*−2), P_BYBLK(*t*−1), P_BYBLK(*t*); Structure (8,1,1), T_BYBLK(*t*), P_BYBLK(*t*), T_BLT(*t*), P_BLT(*t*), T_HJ(*t*), P_HJ(*t*), T_YQ(*t*), P_YQ(*t*); Structure (16,1,1), T_BYBLK(*t*−1), T_BYBLK(*t*), P_BYBLK(*t*−1), P_BYBLK(*t*), T_BLT(*t*−1), T_BLT(*t*), P_BLT(*t*−1), P_BLT(*t*), T_HJ(*t*−1), T_HJ(*t*), P_HJ(*t*−1), P_HJ(*t*), T_YQ(*t*), T_YQ(*t*−1), P_YQ(*t*−1), P_YQ(*t*); Structure (24,1,1), T_BYBLK(*t*−2), T_BYBLK(*t*−1), T_BYBLK(*t*), P_BYBLK(*t*−2), P_BYBLK(*t*−1), P_BYBLK(*t*), T_BLT(*t*−2), T_BLT(*t*−1), T_BLT(*t*), P_BLT(*t*−2), P_BLT(*t*−1), P_BLT(*t*), T_HJ(*t*−2), T_HJ(*t*−1), T_HJ(*t*), P_HJ(*t*−2), P_HJ(*t*−1), P_HJ(*t*), T_YQ(*t*−2), T_YQ(*t*−1), T_YQ(*t*), P_YQ(*t*−2), P_YQ(*t*−1), P_YQ(*t*)

C calibration, *V* verification

from Central Asia did not perform well and cannot be used to reconstruct the precipitation in the Kaidu River Basin.

4.3 The performance assessment of calibrated and verified runoff

The TLBP-FFNN model is used to model monthly runoff in dependency on temperature and precipitation in the target river. Before training the TLBP-FFNN model, the Pearson correlation coefficients were computed for MAT and MAR as well as for MAP and MAR from the above-mentioned sources for the Kaidu River Basin (Table 5). It shows that all correlation coefficients are significant at the 0.01 confidence level, indicating that MAT and MAP from observation, CRU, and CMIP3 data have significant correlation with MAR at Dashankou station and can be used to be input variables of TLBP-FFNN model for simulation of MAR there. Then, MAR was calibrated and verified at Dashankou station using MAT and MAP of all four meteorological stations from observation, CRU, and CMIP3 data as inputs by TLBP-FFNN model. The structures of (2, 1, 1), (4, 1, 1), (6, 1, 1), (8, 1, 1), (16, 1, 1), and (24, 1, 1) are employed to calibrate and verify MAR. Different structures refer to different input variables (see Table 6). Here, the number of hidden neurons is set to 1 for easy comparison among different structures. In fact, the results are similar for TLBP-FFNN model with the same structure using different numbers of hidden neurons in this study. It can be seen that the TLBP-FFNN model with any one structure performs very well when using observed MAT and MAP as input variables. The performance is also fairly good for TLBP-FFNN model with any one structure when using MAT and MAP from grid data of CRU and CMIP3 as input variables.

The greater the number of input variables, the better the performance of the TLBP-FFNN model, generally. However, the value of *AIC* improves with increase of the number of input variables. Considering model accuracy, complexity, and performance, TLBP-FFNN models with structure
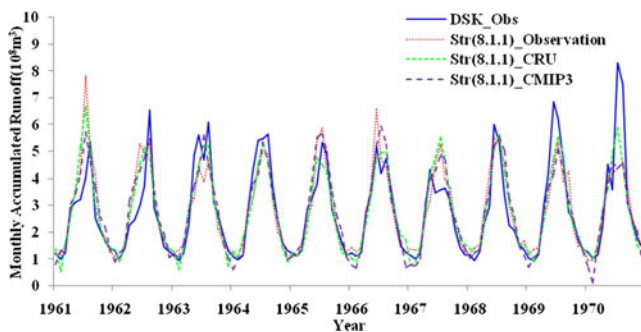
Fig. 5 The time series of observed and verified MAR using TLBP-FFNN model with structure (8,1,1) based on MAT and MAP of four meteorological stations from observation, CRU, and CMIP3 data during verification period (1961–1970) in Kaidu River Basin
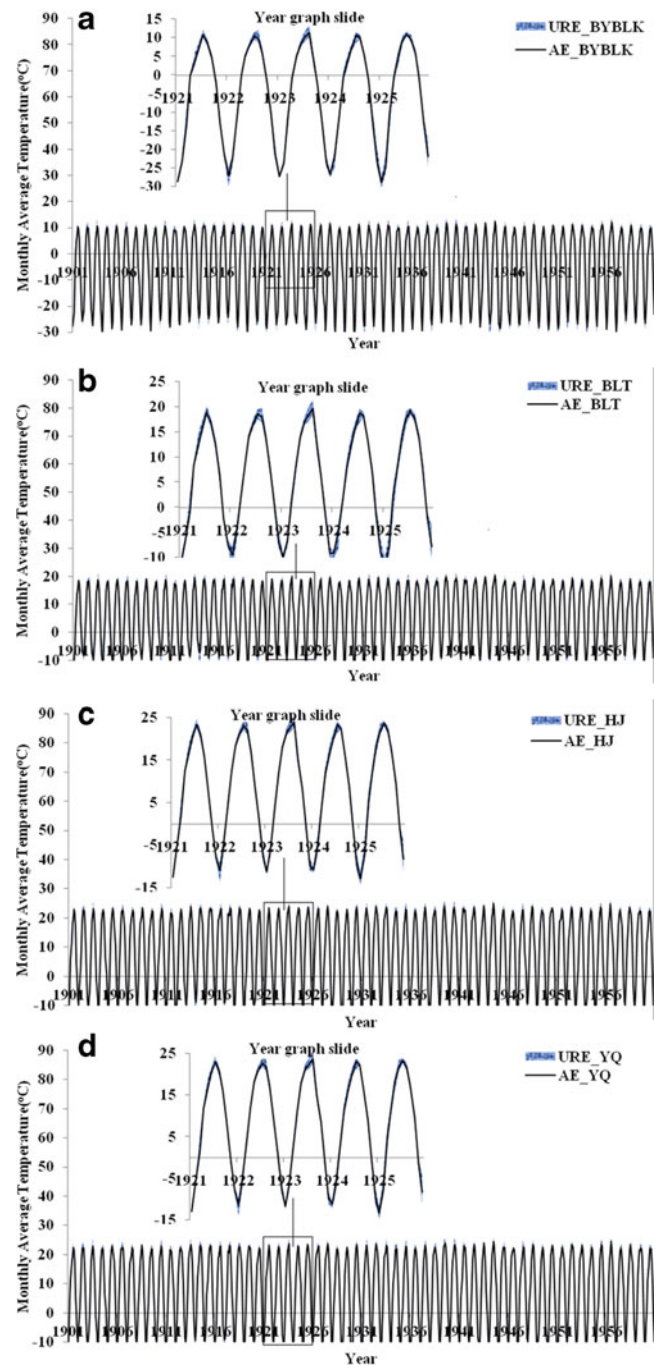

Fig. 6 The time series of MAT reconstructed using Delta method during 1901–1960 in Kaidu River Basin. **a** Bayinbuluke station, **b** Baluntai station, **c** Hejing station, and **d** Yanqi station. The *blue shaded band* denotes the 5 to 95 % uncertainty range estimated (URE) and the *black line* means the average estimated (AE) values

(8,1,1) are the optimal model for calibration and verification of MAR in the Kaidu River Basin. Figure 5 shows the TS of observed and verified MAR using TLBP-FFNN model with structure (8,1,1) based on MAT and MAP of four meteorological stations from observation, CRU, and CMIP3 data during validation period. It demonstrates that the TLBP-

Fig. 7 The time series of MAP reconstructed using Delta method during 1901–1960 in Kaidu River Basin. **a** Bayinbuluke station, **b** Baluntai station, **c** Hejing station, and **d** Yanqi station. The *blue shaded band* denotes the 5 to 95 % uncertainty range estimated (URE) and the *black line* means the average estimated (AE) values
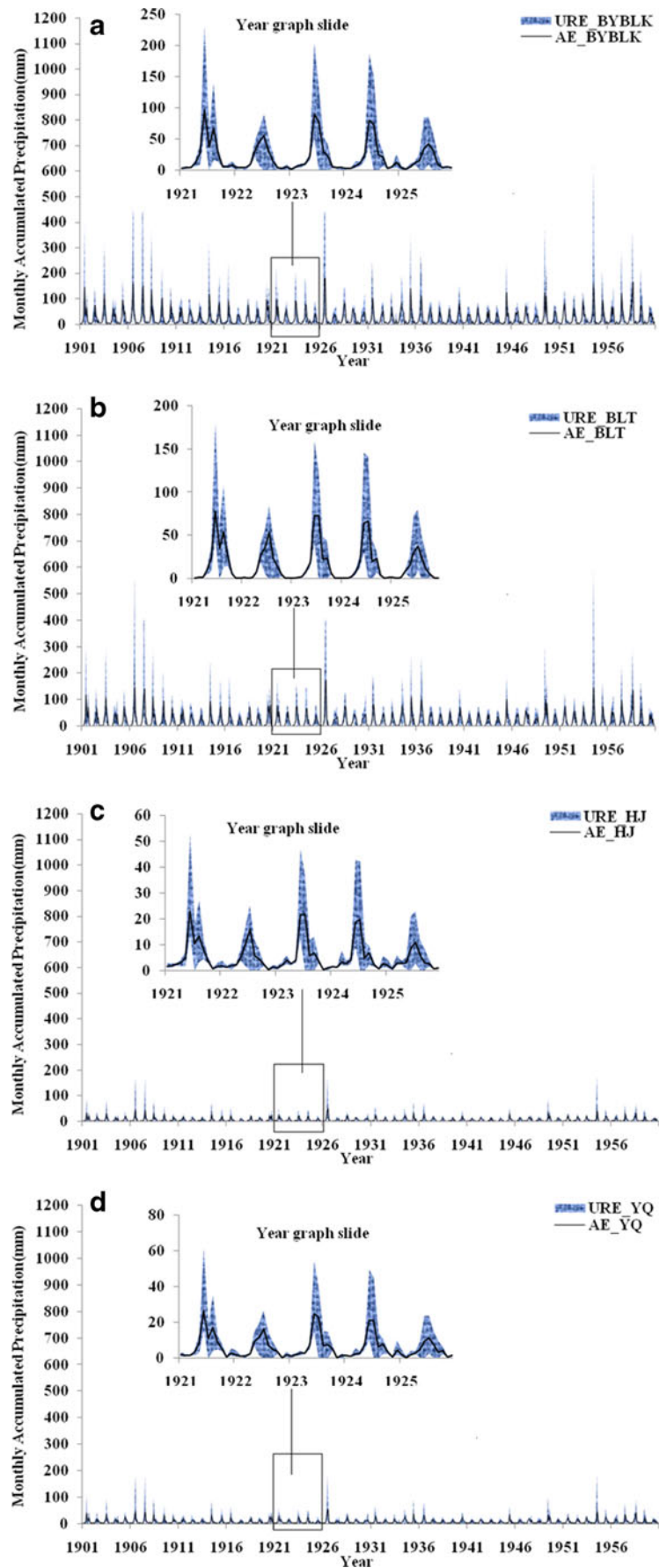
FFNN model with (8, 1, 1) structure trained or tested can catch the runoff variation within a year and numerically reproduce the historical series of runoff but is unable to capture the highest peak of runoff.

4.4 Reconstructions of hydrometeorological parameters and their uncertainty

The reconstructed hydrometeorological TS from 1901 to 1960 are shown in Figs. 6, 7 and 8. Figure 6 shows the reconstructed MAT at four target stations on the basis of three monthly source datasets using the Delta method for the period 1901–1960. The blue shaded band denotes the 5 % to 95 % uncertainty range of six reconstructed TS and the black line is their average estimated (AE) values. It can be seen that the reconstructed TS of MAT captures the annual period well and a small interannual difference during the period of 60 years over all the four target stations. MAT fluctuates periodically and smoothly with uncertainty. The mean of MAT during reconstruction varies from the minimum of -27.82 ± 2.08 °C in January to the maximum of 10.51 ± 1.23 °C in July at Bayinbuluke station (Fig. 6a), -10.40 ± 2.08 °C to 18.66 ± 1.21 °C at Baluntai station (Fig. 6b), -11.87 ± 2.06 °C to 23.13 ± 1.22 °C at Hejing station (Fig. 6c), and -12.23 ± 2.04 °C to 22.80 ± 1.22 °C at Yanqi station (Fig. 6d), respectively. The uncertainty ranges are wider in both the coldest season and the warmest season than other seasons, indicating that there is larger uncertainty in the extreme values of reconstructed MAT. However, the overall uncertainty is quite small from the reconstructed TS of MAT within the four target stations due to the continuity of temperature over the spatiotemporal field.

The TS of MAP reconstructed fluctuates unevenly during the period 1901–1960 over the four target stations (Fig. 7). The annual period and large interannual differences are captured from the TS of MAP reconstructed during the study period over all four stations. The MAP fluctuates periodically and unevenly. The mean of MAP varies from

the minimum of 3.28 ± 1.85 mm in January to the maximum of 69.99 ± 59.83 mm in June at Bayinbuluke station (Fig. 7a), from 0.60 ± 0.33 mm in November to 56.46 ± 58.40 mm in July at Baluntai station (Fig. 7b), from 0.65 ± 0.35 mm in November to 16.90 ± 17.75 mm in July at Hejing station (Fig. 7c), and from 0.83 ± 0.45 mm in November to 18.93 ± 15.95 mm in June at Yanqi station (Fig. 7d). Compared to the MAT, the reconstructed MAP shows a larger uncertainty within a certain year especially in the month of peak value. A larger uncertainty for reconstruction of precipitation might be caused by the discreteness of the precipitation field on the spatial and temporal scales.

Figure 8 shows three reconstructed TS of MAR at Dashankou station using TLBP-FFNN model with structure (8,1,1) fed with the MAT and MAP at the four target stations from reconstruction, CRU, and CMIP3 data during 1901 to 1960. It seizes the annual fluctuation pattern and interannual difference of MAR in the period of 60 years. The mean of MAR changes from low flow with $1.23\times10^8\,\text{m}^3$ in January to peak flow with $5.46\times10^8\,\text{m}^3$ in July based on MAT and MAP from reconstruction, from $0.97\times10^8\,\text{m}^3$ in February to $5.81\times10^8\,\text{m}^3$ in July based on MAT and MAP from CRU data and from $0.85\times10^8\,\text{m}^3$ in January to $5.49\times10^8\,\text{m}^3$ in July based on MAT and MAP from CMIP3 data. The TS of MAR reconstructed based on MAT and MAP from CRU data is similar to that based on MAT and MAP from CMIP3 data and fluctuates periodically and smoothly. However, the TS of MAR reconstructed based on reconstructed MAT and MAP above fluctuates unevenly and presents some high peak values.

4.5 The change and variation of hydrometeorological parameters during the 20th century

TS of reconstructed values from 1901 to 1960 and the observed values from 1961 to 2000 of annual average temperature (AAT) at the four target stations are shown in Fig. 9. The fluctuation of AAT exists over the entire 20th

Fig. 8 The time series of MAR reconstructed based on MAT and MAP from reconstruction, CRU, and CMIP3 data using TLBP-FFNN with structure (8,1,1) during 1901–1960 in Kaidu River Basin
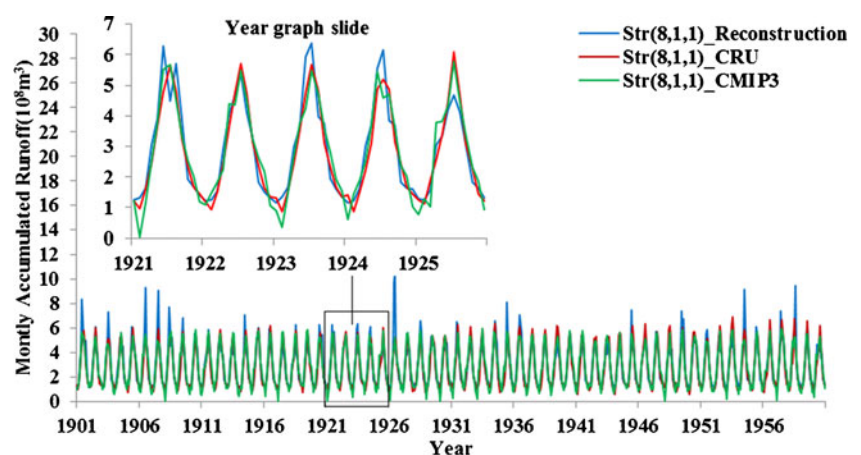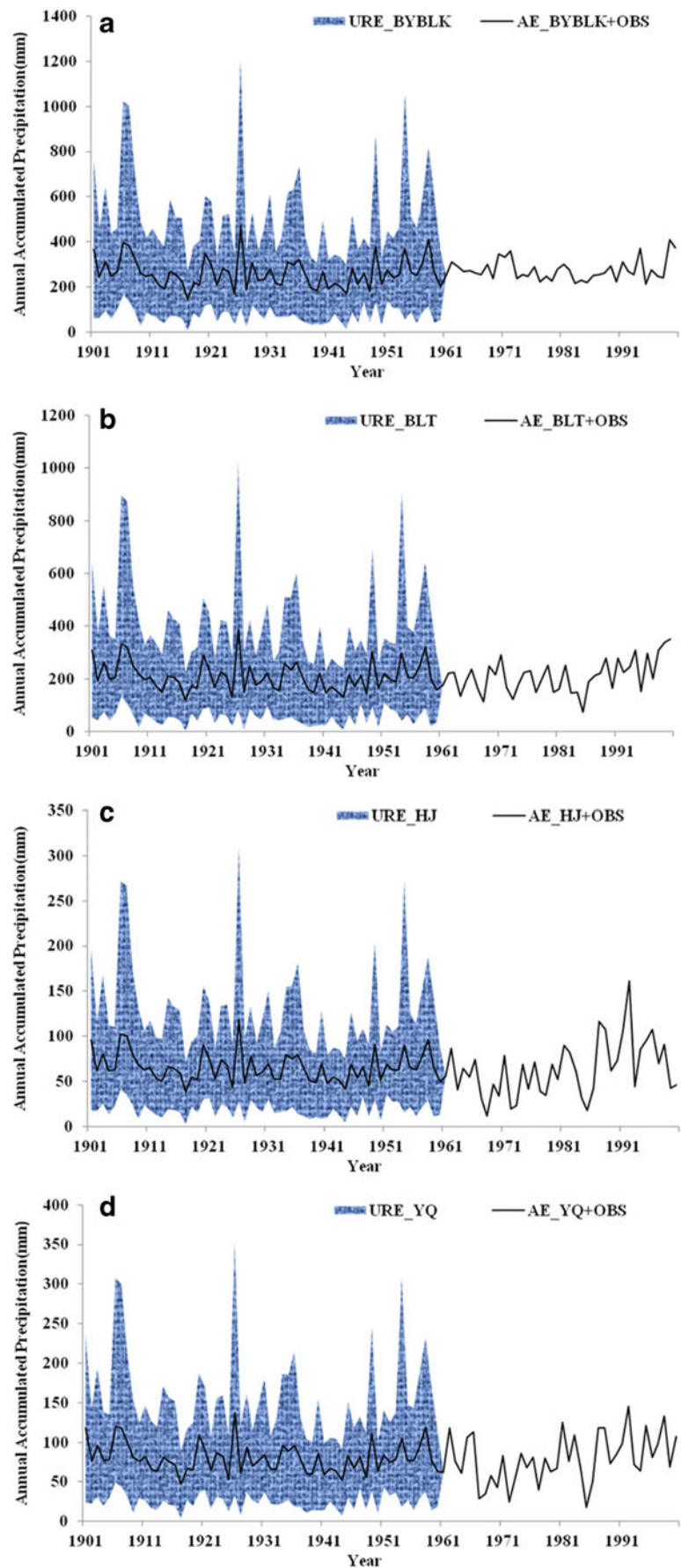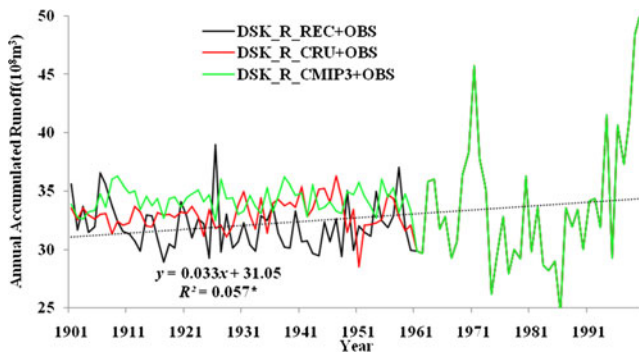
Fig. 9 The time series of AAT over the 20th century in Kaidu River Basin. The 5 to 95 % uncertainty range estimated (URE), average estimated (AE) values during 1901–1960, and the observed (OBS) values during 1961–2000 are linked together and drawn on figures. **a** Bayinbuluke station, **b** Baluntai station, **c** Hejing station, and **d** Yanqi station. The *black dashed line* is the trend line. ** trend is significant at the 0.01 confidence level (two-tailed)
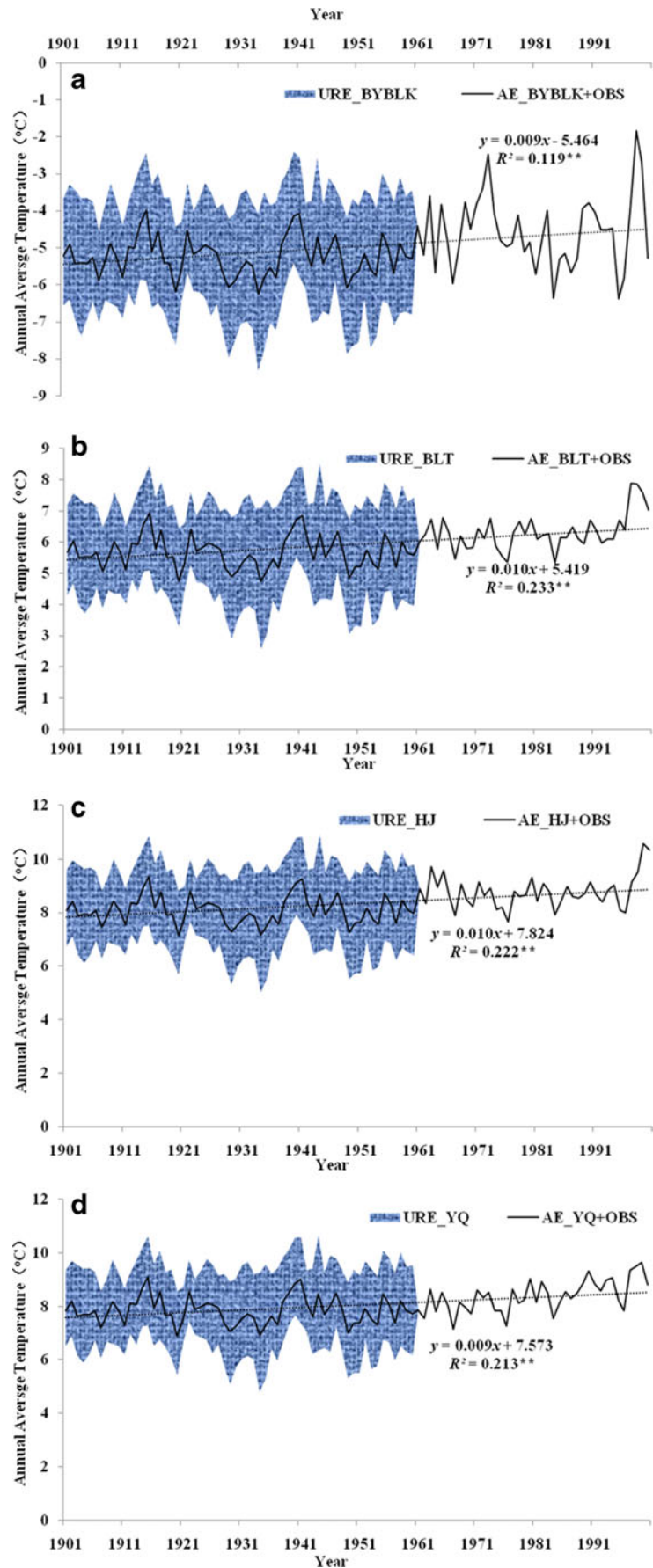
Fig. 10 The time series of AAP over the 20th century in Kaidu River Basin. The 5 to 95 % uncertainty range estimated (URE), average estimated (AE) values during 1901–1960, and the observed (OBS) values during 1961–2000 are linked together and drawn on figures. **a** Bayinbuluke station, **b** Baluntai station, **c** Hejing station, and **d** Yanqi station

Fig. 11 Three time series of AAR over the 20th century in Kaidu River Basin. AAR reconstructed based on MAT and MAP from reconstruction, CRU, and CMIP3 data using TLBP-FFNN with structure (8,1,1) and the observed (OBS) values during 1961–2000 are linked together and drawn on figures. The *black dashed line* is the trend line. * trend is significant at the 0.05 confidence level (two-tailed)

century and shapes of the fluctuation are similar during 1901–1960 for all four target stations (Fig. 9). Trend analysis shows that the whole TS of AAT (average estimated values during 1901–1960 and observed values during 1961–2000) at the four target stations show significant increasing trends at the 0.01 confidence level over the 20th century. The rates of increase are 0.09 °C/10a at Bayinbuluke station (Fig. 9a), 0.10 °C/10a at Baluntai station (Fig. 9b), 0.10 °C/10a at Hejing station (Fig. 9c), and 0.09 °C/10a at Yanqi station (Fig. 9d), respectively. So the temperature of the Kaidu River Basin increased during the 20th century. This is consistent with the conclusions from the IPCC report (Le Treut et al. 2007). However, there are no significant trends during first half century in the 20th century, and the warming happen during the last 40 years of 20th century. So the time scale of climate warming is decadal but not centennial.

Similar to the AAT, large fluctuation exists over both the reconstructed period and the observed period for annual accumulated precipitation (AAP) and shapes of fluctuation are similar during 1901–1960 for all four target stations (Fig. 10). The linked TS of AAP (average estimated values during 1901–1960 and observed values during 1961–2000) at the four target stations present no significant trends over the 20th century. However, Baluntai station, Hejing station, and Yanqi station have significant increasing trends during 1961–2000. It indicates the time scale of climate wetting is also decadal but not centennial.

For annual accumulated runoff (AAR), the three TS at Dashankou station are linked by AAR values reconstructed based on MAT and MAP of four meteorological stations from reconstruction, CRU, and CMIP3 data, respectively, using TLBP-FFNN with structure (8,1,1) during 1901–1960 and the observed values during 1961–2000. The result showed a smoother and steadier curve during the reconstructed period than during the observed period (Fig. 11). Among these three TS, only the linked TS of AAR reconstructed based on MAT

and MAP of the four meteorological stations from reconstruction during 1901–1960 and the observed values during 1961–2000 presents a significant increasing trend with a rate of $0.33 \times 10^8 \, \text{m}^3/10\text{a}$ at the 0.05 confidence level. Similar to AAT and AAP, it shows no significant trends during first half century in the 20th century. Therefore, the change of runoff is also decadal and not centennial.

5 Conclusions

Through collecting available observation data around the neighboring region and grid data from CRU and CMIP3 datasets, this paper extends the starting year of TS of MAT and MAP in the Kaidu River Basin to 1901 using the Delta method. Then, the TLBP-FFNN model is applied to reconstruct the MAR by taking the reconstructed MAT and MAP of the four meteorological stations from reconstruction, CRU, and CMIP3 data as model inputs. The conclusions are as follows:

The Delta method generates satisfactory and similar performance for calibrated and verified MAT in the Kaidu River Basin based on the selected three sources data from 1961 to 2000. The performances based on grid data from CMIP3 and station data from Central Asia are better than grid data from CRU. The calibration and verification of MAP do not perform as well as those of MAT do in four target stations in the Kaidu River Basin, but satisfactory MAP at Bayinbuluke station is obtained based on CRU and CMIP3, in which the CMIP3 data produces better results than those from CRU. So the Delta method can be applied to reconstruct the MAT in the Kaidu River Basin based on the selected three data sources and MAP at Bayinbuluke station based on CRU and CMIP3 data. The MAR from 1961 to 2000 is well calibrated and verified using the TLBP-FFNN model with six structures by taking MAT and MAP at four target stations from observation, CRU, and CMIP3 data, respectively, during 1901 to 1960 as inputs. Considering model accuracy, complexity, and performance, TLBP-FFNN models with structure (8,1,1) are optimal models with good performance for calibration and verification of MAR at Dashankou station in the Kaidu River Basin.

The good performance shown by calibration and verification of the three hydrometeorological variables during 1961–2000 makes it credible to reconstruct the TS of the hydrometeorological parameters during 1901–1960 using the calibrated and verified Delta method and TLBP-FFNN model. The reconstructed TS of MAT, MAP, and MAR capture the characteristic of annual periodicity during the period 1901–1960 well over target stations, but the high frequency signals are difficult to be obtained. The linked TS of AAT, AAP, and AAR based on the reconstruction during 1901–1960 and the observation during 1961–2000 show that the climate in the Kaidu River Basin had changed during the 20th century.

However, it mainly embodies on the decadal climate warming during 1961–2000.

This study showed that the temperature and precipitation correlated significantly with runoff in the Kaidu River Basin. Runoff during unrecorded period can, therefore, be reconstructed based on available temperature and precipitation from selected data sources. Also, the expanded TS can be used to identify the variation or change of water resources for longer time scales under a given uncertainty which is caused by the quality of data sources, reconstruction methods, and other factors. In order to reduce uncertainty, future research should concentrate on collecting extensive and reliable data, selecting better reconstruction methods, and continue searching for environmental factors that impact runoff generation.

References

Akaike H (1974) A new look at the statistical model identification. IEEE Trans Autom Control 19:716–723

ASCE Task Committee on Application of Artificial Neural Networks in Hydrology (2000) Artificial neural networks in hydrology I: hydrology application. J Hydrol Eng 5(2):124–137

Bradley RS, Jones PD (1992) Climate since AD1500. Routledge, London, pp 511–537

Busuioc A, Chen D, Hellstrom C (2001) Performance of statistical downscaling models in GCM validation and regional climate change estimates: application for Swedish precipitation. Int J Climatol 21:557–578

Cannas B, Fanni A, See L, Sias G (2006) Data preprocessing for river flow forecasting using neural networks: wavelet transforms and data partitioning. Phys Chem Earth 31:1164–1171

Chapman L, Thornes JE (2003) The use of geographical information systems in climatology and meteorology. Prog Phys Geogr 27: 313–330

Chen YN, Xu CC, Hao XM, Li WH, Chen YP, Zhu CG, Ye ZX (2009) Fifty-year climate change and its effect on annual runoff in the Tarim River Basin, China. Quat Int 208:53–61, in Chinese

Conway D, Wilby RL, Jone PD (1996) Precipitation and air flow indices over the British Isles. Clim Res 7(2):169–183

Dou Y, Chen X, Bao AM, Li LH (2011) The simulation of snowmelt runoff in the ungauged Kaidu River Basin of TianShan Mountains, China. Environ Earth Sci 62(5):1039–1045

Dubrovsky M, Buchtele J, Zalud Z (2004) High-frequency and low-frequency variability in stochastic daily weather generator and its effect on agricultural and hydrologic modeling. Clim Chang 63:145–179

Esper J, Cook ER, Schweingruber FH (2002) Low-frequency signals in long tree-ring chronologies for reconstructing past temperature variability. Science 295:2250–2253

Fang KY, Gou XH, Chen FH (2011) Large-scale precipitation variability over Northwestern China inferred from tree rings. J Clim 24 (13):3457–3468

Fowler HJ, Kilsby CG, O'Connell PE (2000) A stochastic rainfall model for the assessment of regional water resource systems under changed climatic conditions. Hydrol Earth Syst Sci 4:261–280

Gupta HV, Sorooshian S, Yapo PO (1999) Status of automatic calibration for hydrologic models: comparison with multilevel expert calibration. J Hydrol Eng 4(2):135–143

Hao ZH, Li L, Xu Y, Ju Q (2009) Study on Delta-DCSI downscaling method of GCM output. J SiChuan Univ (Eng Sci Ed) 41(5):1–7, in Chinese

Hay LE, Wilby IL, Leavesley GH (2000) A comparison of delta change and downscaled GCM scenarios for three mountainous basins in the United States. J Am Water Resour Assoc 36(2):387–397

Huth R (1999) Statistical downscaling in central Europe: evaluation of methods and potential predictors. Clim Res 13:91–101

Jeffrey SJ, Carter JO, Moodie KB, Beswick AR (2001) Using spatial interpolation to construct a comprehensive archive of Australian climate data. Environ Model Softw 16:309–330

Karl TR, Wang WC, Schlesinger ME, Knight RW, Portman D (1990) A method of relating general circulation model simulated climate to observed local climate. Part I: seasonal statistics. J Clim 3:1053–1079

Le Treut H, Somerville R, Cubasch U, Ding YH, Mauritzen C, Mokssit A, Peterson T, Prather M (2007) Historical overview of climate change. In: Solomon S, Qin D, Manning M, Chen Z, Marquis M, Averyt KB, Tignor M, Miller HL (eds) Climate change 2007: the physical science basis. Contribution of working group I to the Fourth Assessment Report of the Intergovernmental Panel on Climate Change. Cambridge University Press, Cambridge

Levenberg K (1944) A method for the solution of certain non-linear problems in least squares. Q Appl Math 2:164–168

Li XM, Jiang FQ, Li LH, Wang GG (2011a) Spatial and temporal variability of precipitation concentration index, concentration degree and concentration period in Xinjiang province, China. Int J Climatol 31:1679–1693

Li XM, Li LH, Guo LP, Zhang FY, Suwannee A, Shang M (2011b) Impact of climate factors on runoff in the Kaidu River watershed: path analysis of 50-year data. J Arid Land 3(2):132–140

Marquardt D (1963) An algorithm for least-squares estimation of nonlinear parameters. SIAM J Appl Math 11(2):431–441

Marquinez J, Lastra J, Garcia P (2003) Estimation models for precipitation in mountainous regions: the use of GIS and multivariate analysis. J Hydrol 270:1–11

Mason SJ (2004) Simulating climate over Western North America using stochastic weather generators. Clim Chang 62:155–187

May RJ, Maier HR, Dandy GC (2009) Data splitting for artificial neural networks using SOM-based stratified sampling. Neural Netw 23:283–294

Moriasi DN, Arnold JG, Van Liew MW, Bingner RL, Harmel RD, Veith TL (2007) Model evaluation guidelines for systematic quantification of accuracy in watershed simulations. Am Soc Agric Biol Eng 50(3):885–900

Nash JE, Sutcliffe JV (1970) River flow forecasting through conceptual models. Part 1: a discussion of principles. J Hydrol 10 (3):282–290

Ninyerola M, Pons X, Roure MJ (2000) A methodological approach of climatologically modeling of air temperature and precipitation through GIS techniques. Int J Climatol 20:1823–1841

Nourani V, Komasi M, Mano A (2009) A multivariate ANN-wavelet approach for rainfall–runoff modeling. Water Resour Manage 23:2877–2894

Olsson J, Uvo CB, Jinno K, Kawamura A, Nishiyama K, Koreeda N, Nakashima T, Morita O (2004) Neural networks for rainfall forecasting by atmospheric downscaling. J Hydrol Eng 9(1):1–12

Shen J, Zhang EL, Xia WL (2001) Records from lake sediments of the Qinghai Lake to mirror climatic and environmental changes of the past about 1000 years. Quat Sci 21(6):508–514, in Chinese

Shi YF, Shen YP, Hu RJ (2002) Preliminary study on signal, impact and foreground of climatic shaft from warm-dry to warm-wet in Northwestern China. J Glaciol Geocryol 24:219–226, in Chinese

Skirvin SM, Marsh SE, McClaranw MP, Mekoz DM (2003) Climate spatial variability and data resolution in a semi-arid watershed, south-eastern Arizona. J Arid Environ 54:667–686

Srinivasulu S, Jain A (2006) A comparative analysis of training methods for artificial neural network rainfall–runoff models. Appl Soft Comput 6:295–306

Tao H, Wang GY, Shao C, Song YD, Zou SP (2007) Climate change and its effects on runoff at the headwater of Kaidu River. J Glaciol Geocryol 29(3):413–417, in Chinese

Tao H, Gemmer M, Bai YG, Su BD, Mao WY (2011) Trends of streamflow in the Tarim River Basin during the past 50 years: human impact or climate change? J Hydrol 400:1–9

Tripathi S, Srinivas VV, Nanjundiah RS (2006) Downscaling of precipitation for climate change scenarios: a support vector machine approach. J Hydrol 330:621–640

Vogl TP, Mangis JK, Rigler AK, Zink WT, Alkon DL (1988) Accelerating the convergence of the backpropagation method. Biol Cybern 59:257–263

Wilby RL, Hay LE, Leavesley GH (1999) A comparison of downscaled and raw GCM output: implications for climate change scenarios in the San Juan River basin, Colorado. J Hydrol 225(1–2):67–91

Wu ZT, Zhang HJ, Krause CM, Cobb NS (2010) Climate change and human activities: a case study in Xinjiang, China. Clim Chang 99:457–472

Xu JH, Ji MH, Lu F (2008) Climate change and its effects on runoff of Kaidu River, Xinjiang, China: a multiple time-scale analysis. Chin Geogr Sci 18(4):331–339, in Chinese

Yang B, Braeuning A, Johnson KR, Shi YF (2002) General characteristics of temperature variation in China during the last two millennia. Geophys Res Lett 29:1029–1040

Zhao FF, Xu ZX (2007) Comparative analysis on downscaled climate scenarios for headwater catchment of yellow river using SDS and Delta methods. Acta Meteorol Sin 65(4):653–662, in Chinese

Zorita E, Storch HV (1999) The analog method as a simple statistical downscaling technique: comparison with more complicated methods. J Clim 12:2474–2489